(Received 31 December 2024, Accepted 12 February 2025, Scheduled 15 February 2025)

Broadband Eight-Element MIMO Antenna with High Isolation for 5G Smartphone Applications

Zhonggen Wang[1], Shunqi Liu[1,*], Wenyan Nie[2], Ming Yang[3], and Chenlu Li[4]

[1]*School of Electrical and Information Engineering, Anhui University of Science and Technology, Huainan 232001, China*
[2]*School of Mechanical and Electrical Engineering, Huainan Normal University, Huainan 232001, China*
[3]*School of Electrical and Communications Engineering, West Anhui University, Lu'an 237012, China*
[4]*School Electrical and Information Engineering, Hefei Normal University, Hefei 230061, China*

ABSTRACT: To satisfy the demand for 5G communication to smartphone terminal antennas in element quantity and isolation, an eight-element broadband MIMO antenna system with high isolation is proposed in this paper. The antenna element consists of an L-shaped feed line and a rectangular slot with an open slot. Meanwhile, a stepped impedance tuning structure was integrated within the rectangular slot to optimize broadband impedance matching and expand the operational bandwidth. In addition, a Chinese character "工"-shaped defective ground structure has been innovatively designed to reduce surface wave coupling on the ground plane, achieving an isolation level of over −15 dB. Furthermore, eight antenna elements and six defective ground structures are symmetrically distributed along the long edges of the substrate, with coupling feeding performed through the L-shaped feed lines. The proposed antenna system ultimately achieves an operating bandwidth of 3.4–6.5 GHz below −10 dB, with a total efficiency greater than 90% and an envelope correlation coefficient of less than 0.016. The stability of the system in overlay screen mode, as well as in single-handed and dual-handed smartphone operation modes, is also demonstrated to showcase its practical applications.

1. INTRODUCTION

Due to the rapid development of science and technology, mobile communication has evolved from the 2G era to the 5G era [1]. Compared to previous mobile terminal communication technologies, 5G has higher requirements for information transmission rate. According to communication system theory, the larger the channel capacity is, the higher the information transmission rate is. In this regard, multiple-input multiple-output (MIMO) antenna design can enhance channel capacity and minimize the impact of multipath effects. By increasing the number of antenna elements in the MIMO system, a high information transmission rate that meets 5G communication requirements can be achieved. Under Rayleigh fading channel conditions, the ergodic channel capacity of an 8×8 MIMO system can reach a maximum value of 46 bps/Hz at a signal-to-noise ratio of 20 dB [2]. Compared to the maximum value of 11.4 bps/Hz achievable by a dual-element MIMO system, the channel capacity of an 8×8 MIMO system is approximately four times of that amount. The antenna proposed in this paper is also designed based on MIMO technology.

Furthermore, MIMO systems for 5G smartphones should also possess broadband characteristics. According to the 3G partnership project technical specification 38.101, the key deployment bands for 5G networks within the Sub-6 GHz frequency range are n77 (3300 MHz–4200 MHz), n78 (3300 MHz–3800 MHz), and n79 (4400 MHz–5000 MHz) [3]. Among the MIMO antenna systems [4–24] proposed for 5G smartphones over the past few years, [4–16] represent single-band MIMO antenna systems with insufficient bandwidth to meet practical applications due to their narrow bandwidth. In contrast, [17–24] are broadband MIMO antenna systems, proposed with the aim of further covering the Sub-6 GHz band. However, it is noteworthy that these antennas were not designed with consideration for the 6 GHz band. The 6 GHz band (5925 MHz–7125 MHz), as an important component of mid-band frequency, has received extensive attention in recent years. This band combines the coverage advantages of low-band frequency with the capacity advantages of high-band frequency, enabling the contiguous allocation of multi-gigahertz wideband spectrum. It is the optimal candidate band for wide-area, high-capacity connectivity. Currently, many countries and regions around the world are studying plans and usage schemes for the 6 GHz band to support the development of 5G and future 6G systems.

Compared to the 6 GHz band, which is currently under research, Sub-6 GHz is the mainstream band for MIMO antenna design. Recently, various smartphone antennas for the Sub-6 GHz frequency band have been reported in literature [25–28]. In [25], a dual-L-shaped slot antenna etched on a metal ground plane is proposed, which enhances the antenna capacitance and improves impedance matching performance through an I-shaped open slot. However, due to the simple design of the antenna structure, [25] only covers the 5G NR bands n77/n78/n79 with a relatively narrow bandwidth. In [26], a MIMO antenna system composed of six identical asymmetric mirror-coupled building blocks is introduced, achieving iso-

* Corresponding author: Shunqi Liu (2024200867@aust.edu.cn).

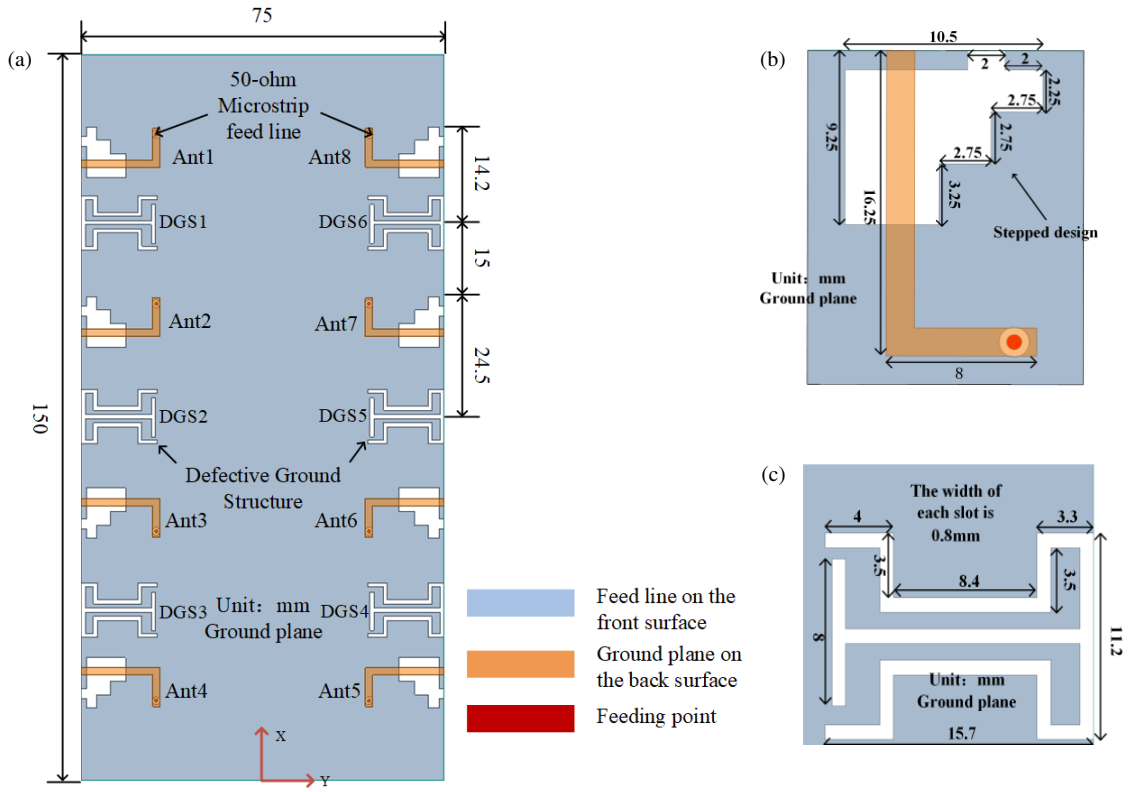

FIGURE 1. Geometry of the proposed MIMO antenna system. (a) Perspective view; (b) Detailed structure of the slot antenna element (taking Ant1 as an example); (c) Detailed structure of the DGS (taking DGS1 as an example).

lation performance exceeding 14 dB without decoupling elements. Nevertheless, compared to an eight-element MIMO antenna system, the six-element system exhibits lower channel capacity and information transmission rate. In [27], eight antenna elements are rationally placed along the long and short edges of the substrate, successfully enabling the MIMO antenna system to operate within the 3.3–6 GHz range through the double coupled-fed loop modes and a slot mode. However, this design does not reserve space for 2G/3G/4G antennas. In [28], a broadband multi-mode antenna is created using an improved L-shaped patch antenna, a gun-shaped slot on the ground plane, and two small stubs protruding from the metal ground plane. Nevertheless, due to the lack of antenna element miniaturization and separate decoupling elements, the isolation performance is relatively low, at only 12.9 dB.

Based on the above discussion, this paper proposes a broadband eight-port slot antenna with high isolation suitable for 5G NR. This design enhances impedance matching performance through slotted openings implemented along the sidewalls of the rectangular slot, while a specialized stepped impedance tuning structure is incorporated at one end of the slot to improve overall antenna performance. In addition, to achieve decoupling, a Chinese character "工"-shaped defective ground structure is designed. Ultimately, the eight antenna elements achieve isolation greater than 15 dB, with an antenna bandwidth of 3.4–6.5 GHz, covering the n77/n78/n79 and WLAN 5-GHz bands. Furthermore, this frequency range also includes a portion of the highly anticipated 6 GHz band, which is significant for the development of 5G and future 6G systems. At the same time, space is reserved on the substrate for 2G/3G/4G antennas to facilitate a smooth transition to 5G communication systems.

2. DESIGN OF PROPOSED MIMO ANTENNA

2.1. Antenna Geometry

The proposed eight-element MIMO antenna is shown in Figure 1(a). Eight antenna elements and six defected ground structures are designed on both sides of the substrate in a symmetric arrangement. The antenna elements are numbered from Ant1 to Ant8. The substrate has a relative dielectric constant of 4.4 and a loss tangent of 0.02, which has dimensions of $15 \times 75 \times 0.8\,\text{mm}^2$ and can be easily utilized in 5.9-inch 5G smartphones. Meanwhile, the antenna element proposed in this design is shown in Figure 1(b) (Taking Ant1 as an example). The L-shaped feed line in the figure is made up of two parts, a $16.25 \times 1.5\,\text{mm}^2$ vertical part and an $8 \times 1.5\,\text{mm}^2$ horizontal part. The proposed rectangular slot also differs from traditional slot antennas. Specifically, this rectangular slot has an open slot with an area of $2 \times 1\,\text{mm}^2$ and features a stepped design. In addition, this design also proposes a symmetric defected ground structure (DGS) to address the issue of mutual coupling between antenna units caused by surface waves on the ground plane, with the specific structure illustrated in Figure 1(c).

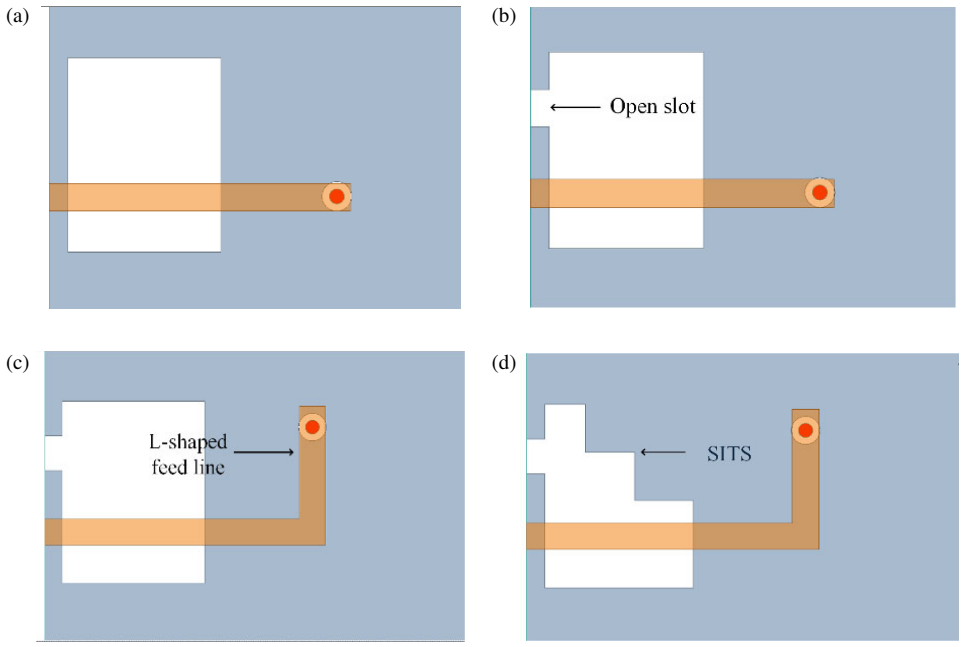

FIGURE 2. Antenna evolution of the suggested scheme. (a) Model 1; (b) Model 2; (c) Model 3; (d) Model 4.

2.2. Design and Analysis

The evolutionary design of the slot antennas is illustrated in Figure 2, with the reflection coefficients of each model shown in Figure 3. Conventional closed/open slot antennas typically exhibit a single resonant mode with narrow bandwidth. To achieve multi-mode resonance and broaden the operating bandwidth, Model 1 adopts a slot width-to-length ratio of 79%, enhancing mode manipulation through increased slot area. However, this widened slot design reduces equivalent capacitance, resulting in degraded impedance matching and no observable resonant modes. To address this, Model 2 introduces an I-shaped open slot to Model 1. The fringing electric fields from the open lot couple with the adjacent ground plane, forming an additional edge capacitance (C_2) to compensate for the main slot capacitance. Simultaneously, the extended current path induced by the open stub excites a suppressed low-frequency resonant mode, successfully achieving a resonance at 3.8 GHz, as shown in Figure 3.

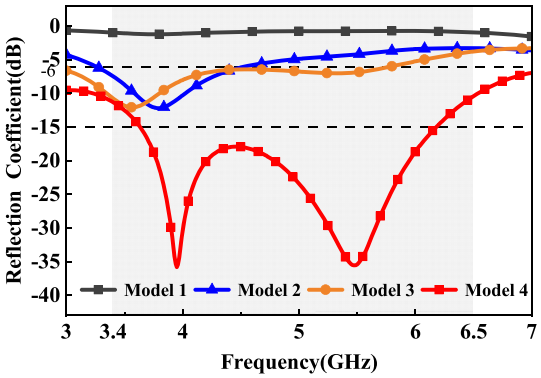

FIGURE 3. The reflection coefficients of models.

Model 3 further replaces the I-shaped feedline with an L-shaped configuration. The bent feedline introduces a series inductance (L_{feed}) and distributed capacitance (C_1). The series inductance (L_{feed}) neutralizes the capacitive impedance component of the antenna, while the distributed capacitance (C_1) counteracts inductive reactance at higher frequencies, significantly expanding the bandwidth to cover the N79 communication band. Building on these advancements, Model 4 incorporates a novel stepped impedance tuning structure (SITS) within the rectangular slot. The SITS induces nonuniform geometric perturbations to reconfigure current distributions, where its stepped profile forces current path bending to excite multi-mode resonance. By precisely adjusting step parameters (height/width), localized electric field coupling strength is controlled to generate tunable capacitive component (C_3), enabling optimized broadband impedance matching. Experimental results demonstrate that the parameterized SITS design flexibly adapts to multi-band requirements. By leveraging mode superposition effects, it achieves a 3.1 GHz bandwidth while preserving structural compactness, with the reflection coefficient (S_{11}) stabilized below -15 dB across the 3.4–6 GHz frequency rang, as shown in Figure 3.

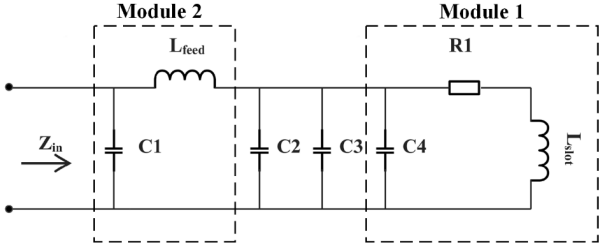

FIGURE 4. The equivalent circuit model of Model 4.

To elucidate the operational mechanism of Model 4 in depth, its equivalent circuit model is illustrated in Figure 4. In this model, the rectangular radiating slot and L-shaped feedline are represented as equivalent circuit Module 1 and Module 2, respectively. Here, C_2 originates from the fringing electric field coupling effect of the open slot, while C_3 corresponds to the tunable capacitive reactance introduced by the SITS. By precisely adjusting the length and width of the SITS steps, the capacitance value of C_3 can be modulated to optimize impedance matching characteristics at resonant points and expand the antenna's operating bandwidth.

2.3. Current Distribution

To facilitate an intuitive analysis of the working principle of the antenna element, the surface currents of Model 4 (placed in the position of Ant1) are examined. As shown in Figure 5, when Model 4 is excited at 3.95 GHz, it exhibits a maximum current distributed at the rectangular end of the slot. The length of the maximum current is 18.5 mm, approximately one-quarter of the wavelength at 3.95 GHz, indicating that the antenna operates in a 0.25λ (corresponding to the wavelength at that frequency) resonant mode at 3.95 GHz. In contrast, when Model 4 operates at 5.5 GHz, the strong currents are mainly distributed at the stepped end of the slot. The length of the strong currents is 25 mm, roughly half of the wavelength corresponding to 5.5 GHz, suggesting that the antenna operates in a half-wavelength resonant mode at 5.5 GHz. The weaker currents are primarily distributed at the rectangular end of the slot.

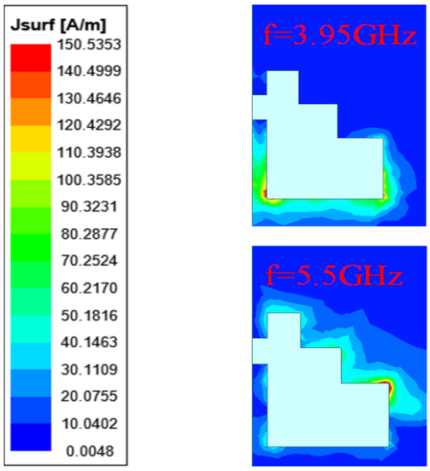

FIGURE 5. Surface current distribution of the antenna element.

MIMO systems, being multi-antenna systems, are bound to cause coupling when being placed in small terminals such as mobile phones. The primary factor causing mutual coupling in this design is the coupling of surface waves on the ground plane. To enhance the isolation between antenna elements, this paper proposes an "工"-shaped defective ground structure (DGS). When DGS1 and DGS2 are etched between Ant1 and Ant2, the simulated isolation is shown in Figure 6. The evolution process of the defective ground structure is illustrated in Figure 7. DGS1 is a T-shaped structure with a relatively short overall slot length. DGS2, based on DGS1, symmetrically

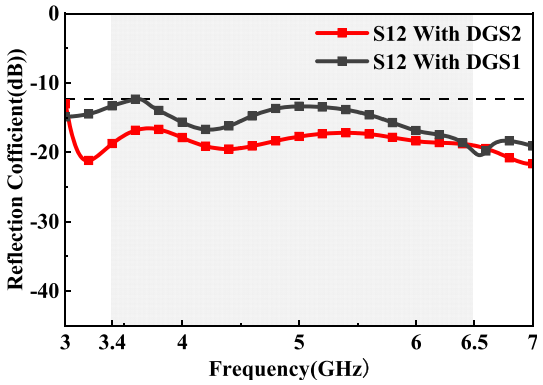

FIGURE 6. Transmission coefficients with and without the defective ground structure (taking S_{23} as an example).

adds two bent slots, forming the shape of the Chinese character "工". In Figure 6, DGS2 exhibits an isolation level higher than 16.5 dB, outperforming DGS1, which shows an isolation level of 12.3 dB. To demonstrate the isolating effect of DGS2, Figures 8(a) and (b) respectively showcase the current distribution on the ground plane with DGS1 and DGS2. By introducing slots with a longer overall length, DGS2 alters the current distribution on the ground plane. Meanwhile, compared to DGS1, the overall longer slots of DGS2 result in more circumferential flow of ground current around it, which reduces the ground current spreading to other ports and enhances the isolation between antenna elements.

3. RESULTS AND DISCUSSION

In this section, with the help of the antenna model shown in Figure 9, an in-depth exploration was conducted on the practical feasibility of the eight-element MIMO antenna system. The core topics of the research included the measured S-parameter values of the MIMO antenna elements, radiation characteristics, and efficiency performance. Meanwhile, the MIMO performance was also evaluated by using envelope correlation coefficient. In the initial stage, the electromagnetic simulation software HFSS was used to model and conduct a detailed analysis on the 8-element slot MIMO antenna system. Subsequently, a vector network analyzer was utilized to accurately measure the S-parameters of the fabricated prototype antenna. In the design of the antenna, the feeding patch was firmly installed on the inner core of the SMA connector, while the ground plane was reliably connected to the outer shell of the SMA connector. Entering the testing stage, the test ports were connected to external devices through cables, and all the unused ports were matched to 50 Ω loads to ensure the accuracy of the tests. In addition, the antenna model was also subjected to relevant far-field measurements in a microwave anechoic chamber, as shown in Figure 10. In the following content, this paper will introduce and analyze in detail the results obtained from these tests.

3.1. S-Parameters

The reflection coefficients (taking Ant1 and Ant2 as examples) and transmission coefficients of the antenna model are presented in Figures 11 and 12. In Figure 11(a), the simulated

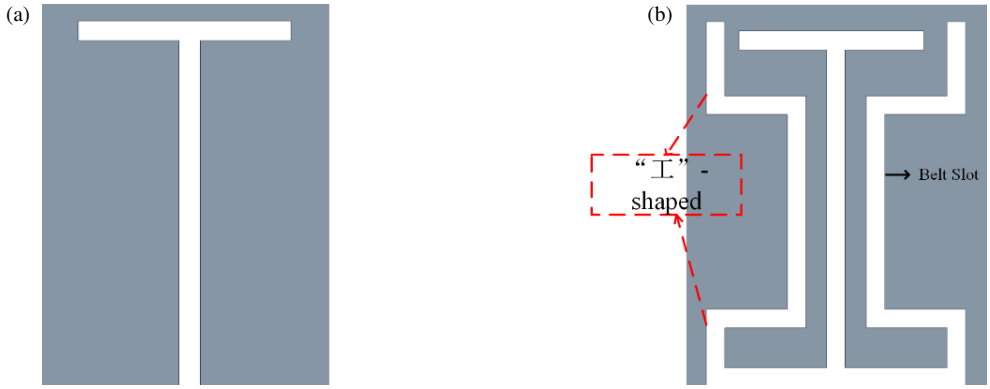

FIGURE 7. Evolution process of the defective ground structure, (a) DGS1; (b) DGS2.

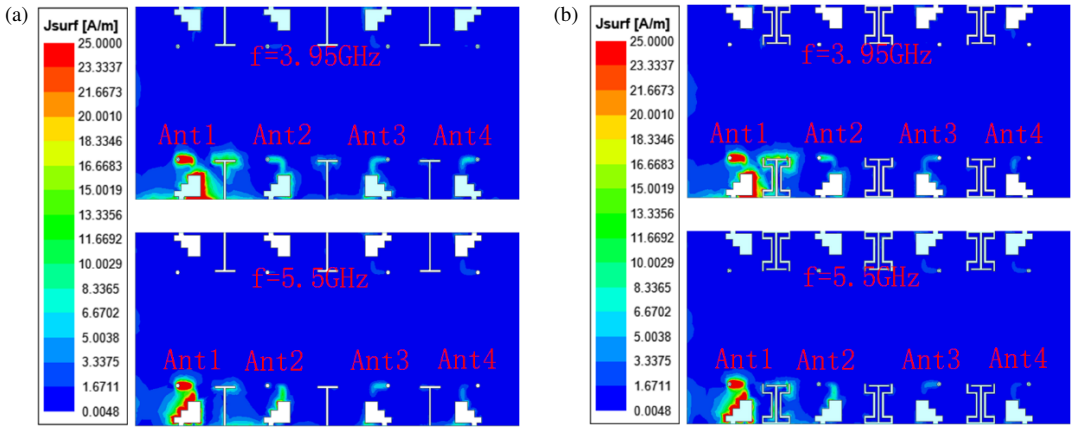

FIGURE 8. Distribution of ground current, (a) with DGS1; (b) with DGS2.

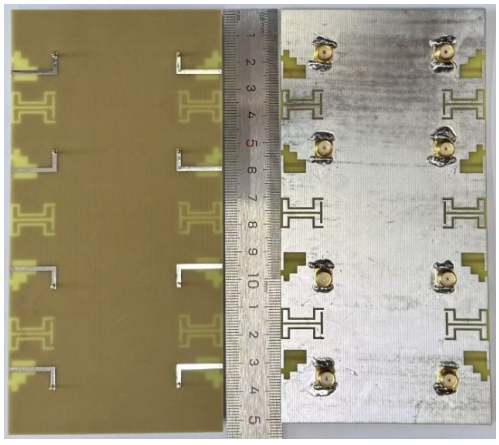

FIGURE 9. Manufactured antenna system.

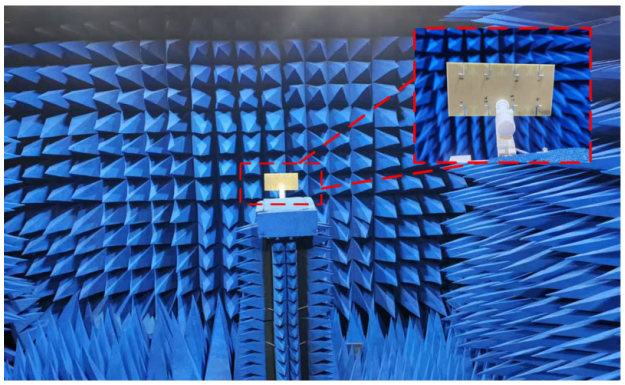

FIGURE 10. Far-field test environment.

bandwidth of the antenna elements is described as ranging from 3.4 GHz to 6.5 GHz. In comparison, within the measured reflection coefficients shown in Figure 11(b), the measured reflection coefficient of Ant1 increases overall within the measured frequency range, while the reflection coefficient of Ant2 increases within the range of 3.6–5.4 GHz, but the reflection coefficients of Ant1 and Ant2 remain below −10 dB, indicating good impedance matching performance. Notably, comparing the measured transmission coefficients in Figure 12(b) with the simulated transmission coefficients in Figure 12(a), S_{12}, S_{13}, S_{14}, and S_{24} all show an increase. However, they still maintain an isolation level of −15 dB within the operating frequency band, meeting the design expectations. Additionally, the discrepancy between simulation and measurement results may be attributed to the losses in SMA connectors and transmission lines.

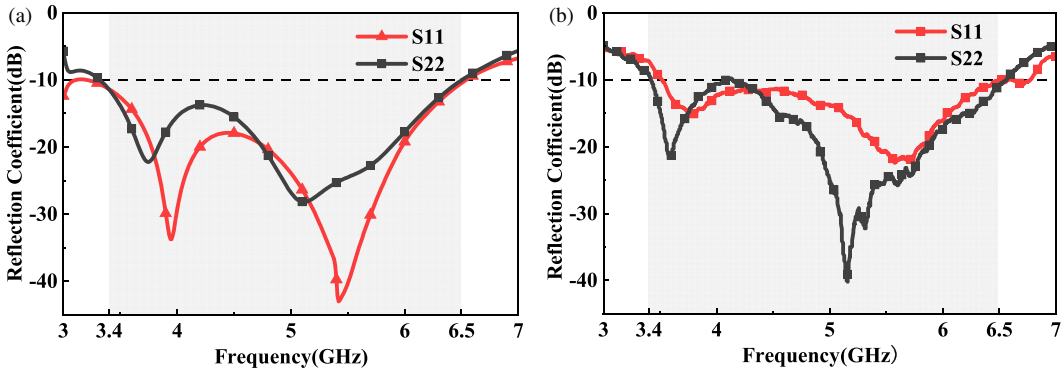

FIGURE 11. The results of reflection coefficients, (a) simulation; (b) measured.

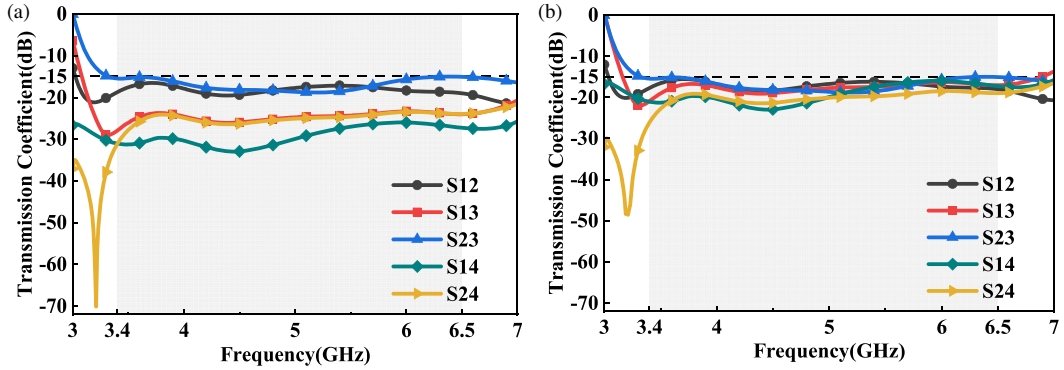

FIGURE 12. The results of transmission coefficients, (a) simulation; (b) measured.

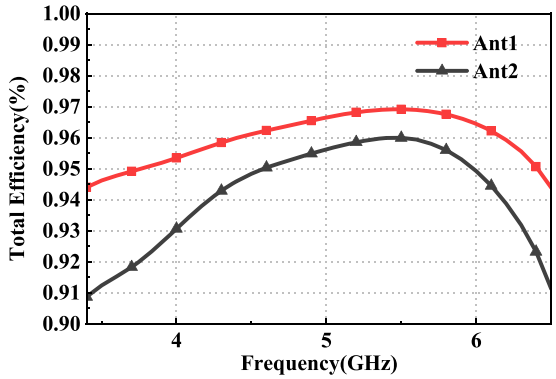

FIGURE 13. Simulated total efficiency values of Ant1 and Ant2.

3.2. Radiation Performance

Figure 13 displays the efficiencies obtained through simulations, with Ant1 and Ant2 as examples. The efficiency of Ant1 ranges from 94% to 97%, while Ant2's efficiency lies between 91% and 96%. Overall, the proposed eight-element MIMO antenna exhibits high radiation efficiency.

Figure 14 presents the simulated and measured radiation patterns of antenna elements Ant1 and Ant2 when they are independently excited in different resonant modes within the XOZ, YOZ, and XOY planes. It can be observed that, at the low-frequency resonant mode, Ant1 (with a resonant frequency of 3.95 GHz) exhibits higher radiation efficiency between 120° and 60° in the XOZ plane, while Ant2 (with a resonant frequency of 3.7 GHz) demonstrates higher radiation efficiency from 120° to 240° and from 300° to 60° in the same plane. Additionally, both Ant1 and Ant2 can effectively produce omnidirectional radiation in the YOZ plane. At the high-frequency resonant mode, Ant1 (with a resonant frequency of 5.5 GHz) and Ant2 (with a resonant frequency of 5 GHz) exhibit good omnidirectional radiation performance in both the XOZ and YOZ planes.

Meanwhile, Ant1 (with a resonant frequency of 3.95 GHz) demonstrates superior radiation performance between 60° and 300° in the XOY plane, while Ant2 (with a resonant frequency of 3.7 GHz) exhibits higher radiation efficiency between 210° and 330° in the same plane. In the high-frequency resonant mode, Ant1 (with a resonant frequency of 5.5 GHz) and Ant2 (with a resonant frequency of 5 GHz) possess more significant radiation performance between 210° and 330° within the XOY plane. However, due to the influence of the testing environment, some inevitable errors exist between the simulations and actual measurements of the two-dimensional radiation patterns of the antennas.

3.3. Envelope Correlation Coefficient

Envelope correlation coefficient (ECC) is a metric that measures the degree of correlation between communication channels. In wireless communication systems, especially MIMO systems, ECC is used to quantify the correlation between antenna element channels. A lower ECC value indicates less cor-

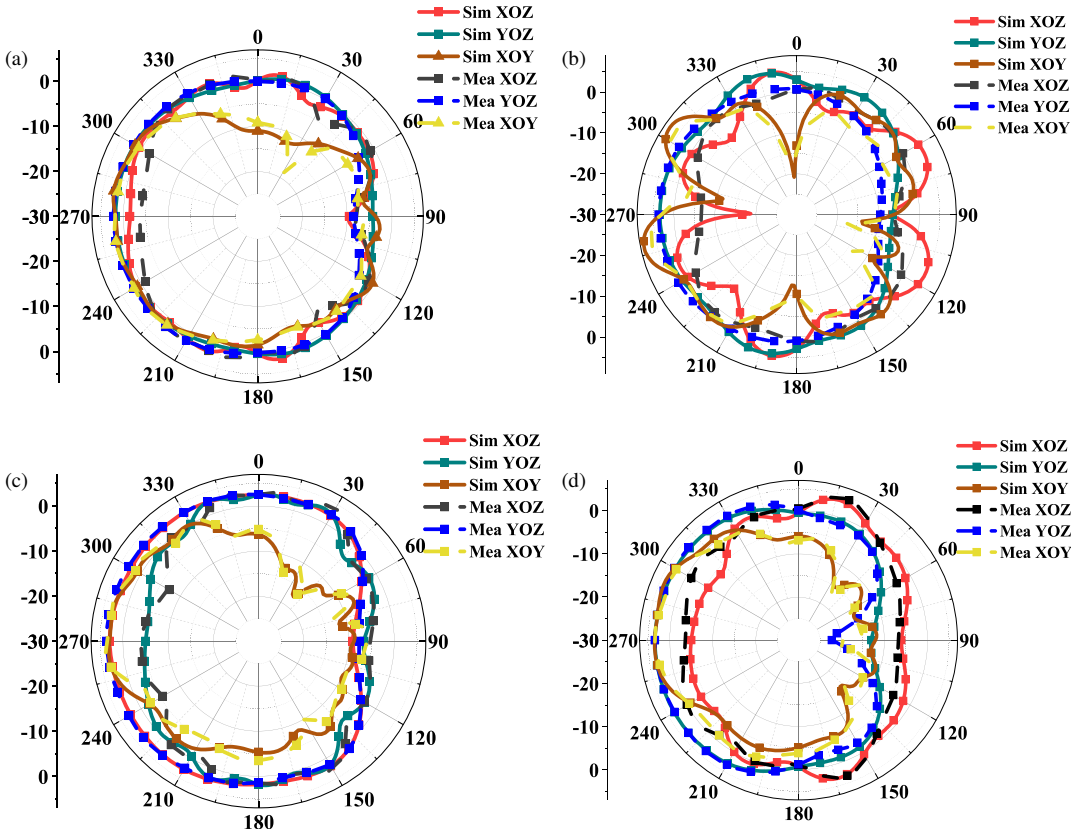

FIGURE 14. Simulated and measured 2D radiation patterns of the proposed MIMO system. (a) Ant1 at 3.5 GHz; (b) Ant2 at 3.7 GHz; (c) Ant1 at 5.5 GHz; (d) Ant2 at 5 GHz.

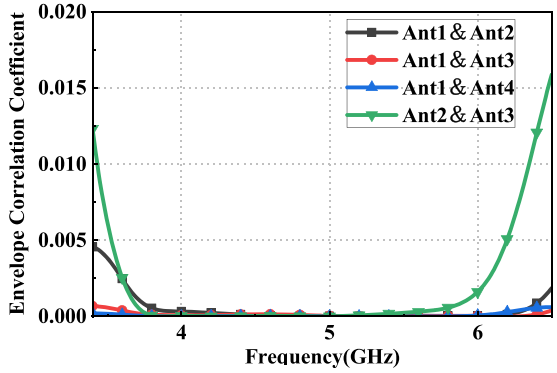

FIGURE 15. Envelope correlation coefficients of MIMO antenna elements.

relation between antennas, which leads to better performance of the MIMO system. As shown in Figure 15, within the operating bandwidth of 3.4 GHz to 6.5 GHz, the ECC values remain below 0.016. Based on comprehensive ECC simulation results, the antenna structure proposed in this paper exhibits commendable diversity performance. ECC can be calculated from S-parameters by using the following formula [28]:

$$\rho_{ij} = \frac{\left|\iint_{4\pi} \bar{F}_i(\theta,\emptyset)\cdot\bar{F}_j^*(\theta,\emptyset)\,d\Omega\right|^2}{\iint_{4\pi}\left|\bar{F}_i(\theta,\emptyset)\right|^2 d\Omega\cdot\iint_{4\pi}\left|\bar{F}_j(\theta,\emptyset)\right|^2 d\Omega} \quad (1)$$

4. PRACTICAL APPLICATION ANALYSIS

This section will investigate the influence of the common single-hand mode (SHM), double-hand mode (DHM), and overlay screen mode on antenna performance. The SHM, DHM, and overlay screen mode are illustrated in Figure 16, while Figures 17, 18, and 19 provide the simulated results of the performance under these three scenarios.

Figure 17(a) shows that the impedance matching performance of Ant2 and Ant3 is degraded due to the obstruction of the palm, and the remaining six antenna elements are not much affected and still cover the required frequency band. Figure 17(b) illustrates that the transmission coefficients between Ant1 and Ant2, and between Ant2 and Ant3, slightly decrease to 14.3 dB. This indicates that the isolation between antenna elements is slightly higher than that without hand interference. Figure 17(c) displays the antenna efficiency after incorporating the hand model, revealing that all antenna elements experience a decrease in efficiency. Among them, Ant3, located at the center of the palm, has its efficiency reduced by approximately 70% due to the simultaneous absorption of electromagnetic waves by the thumb and palm.

Unlike SHM, Figures 18(a) and 18(b) indicate that the antenna reflection coefficients in DHM are not significantly affected by hand tissues. Due to the absorption of electromagnetic waves by both hands, the transmission coefficient between antenna elements increases to 16.3 dB. As shown in Fig-

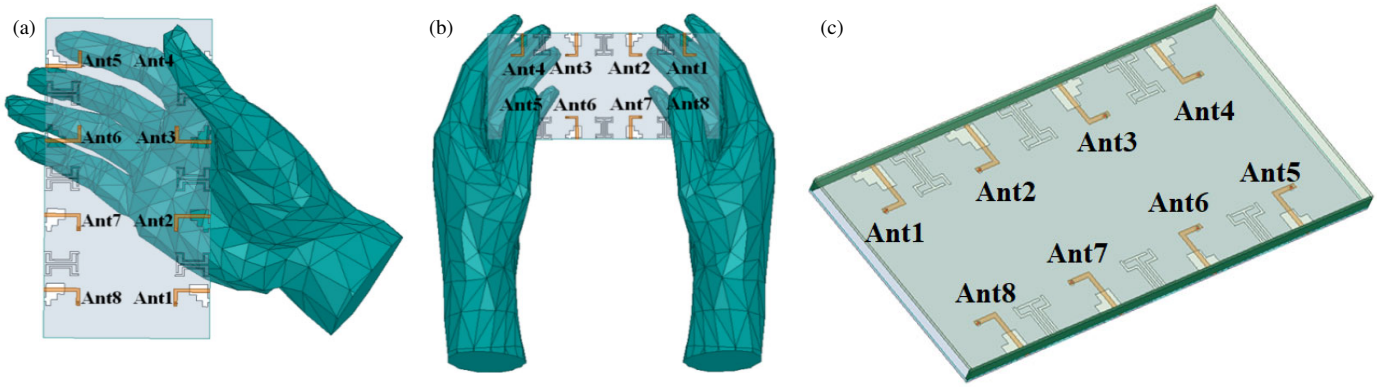

FIGURE 16. Three application scenarios for smartphones. (a) SHM; (b) DHM; (c) Overlay screen.

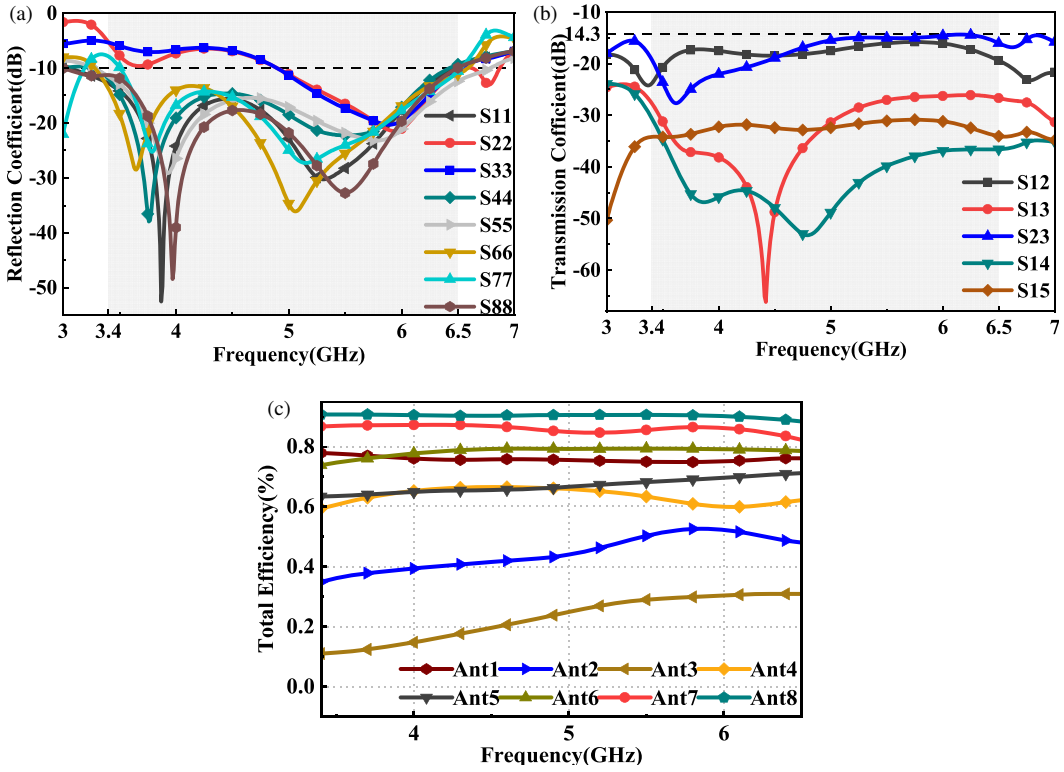

FIGURE 17. Simulated performance parameters in SHM mode. (a) Reflection coefficient; (b) Transmission coefficient; (c) Total efficiency.

ure 16(b), the model for the two-hand mode is symmetrical, resulting in a symmetrical decrease in the efficiency of antenna elements at symmetrical positions. Among them, Ant5 and Ant8 experience the largest decrease in efficiency, approximately 70%, due to being wrapped by the palms.

Since the impact of the overlay screen mode on the antenna elements is symmetrical, the efficiencies of Ant1 and Ant2 are taken as examples in Figure 19. As shown in Figure 19, adding a mobile phone screen causes a shift in the resonant frequency of the antenna elements, resulting in a change in the antenna bandwidth from 3.4–6.5 GHz to 3.1–6.1 GHz. The modified antenna bandwidth still covers the 5G n77/n78/n79 frequency bands. Meanwhile, the isolation between antenna elements remains above 14.4 dB, and the efficiency of all antennas stays above 60%. In summary, the MIMO antennas exhibit excellent performance and high anti-interference capabilities in SHM, DHM, and overlay screen modes.

5. MIMO ANTENNA PERFORMANCE COMPARISON

To validate the superiority of the proposed antenna array, this paper compares the designed array with several previously reported designs, as shown in Table 1. According to MIMO antenna design specifications, the comparison focuses on five aspects: bandwidth, isolation, ECC, overall efficiency values, and antenna size. After comparison, the highlights of this design are as follows. The proposed MIMO antenna system can cover the frequency band of 3.4–6.5 GHz, which is broader than all the antennas mentioned in Table 1. Additionally, the innovatively proposed "工"-shaped DGS in this paper brings excellent isolation performance to the MIMO system, with iso-

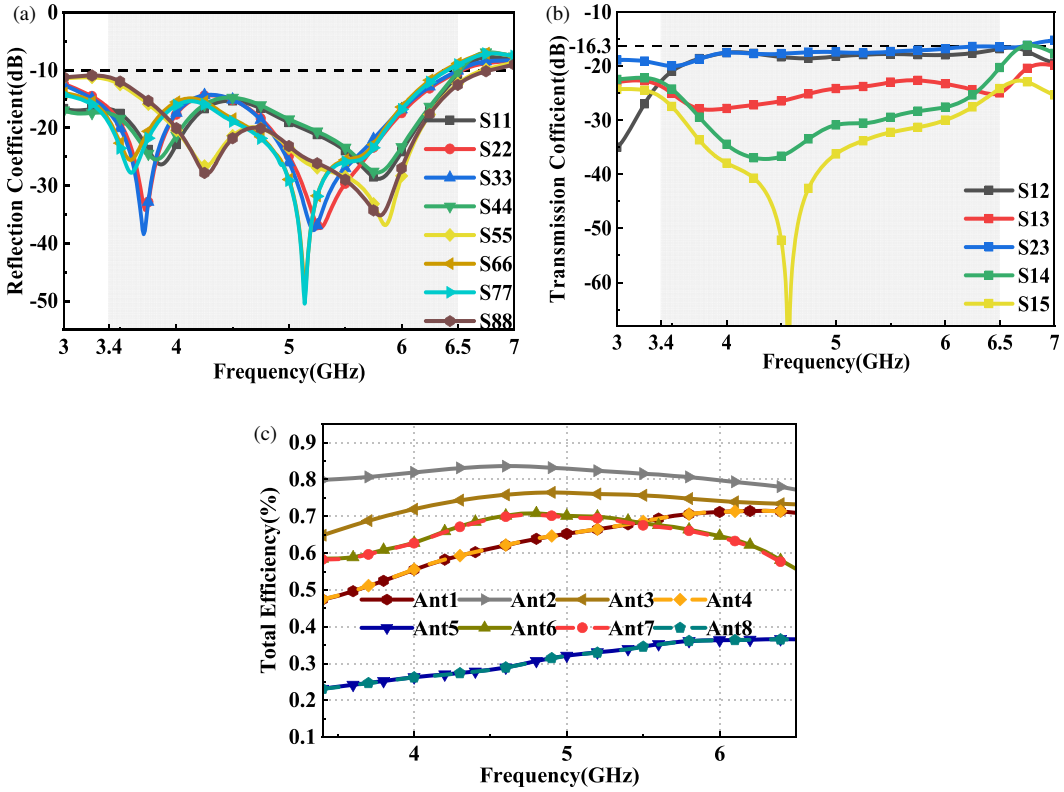

FIGURE 18. Simulated performance parameters in DHM mode. (a) Reflection coefficient; (b) Transmission coefficient; (c) Efficiency.

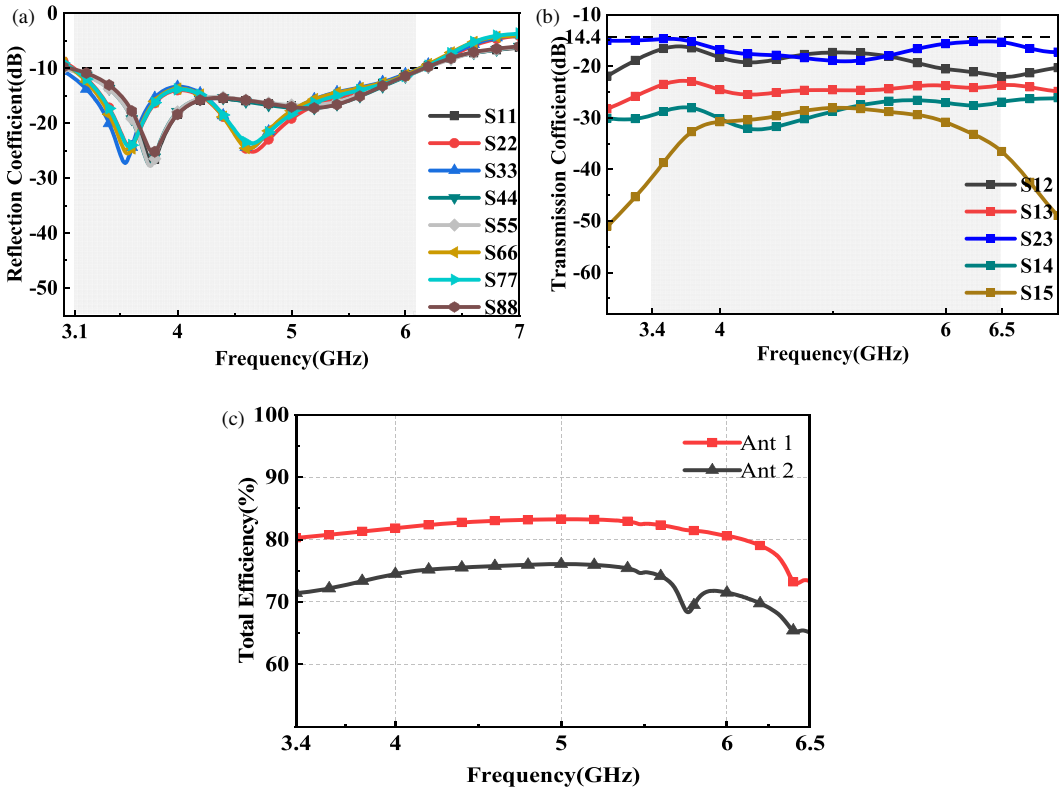

FIGURE 19. Simulated performance parameters under overlay screen mode. (a) Reflection coefficients; (b) Transmission coefficient; (c) Efficiency.

TABLE 1. Antenna performance comparison.

References	Bands (GHz)	Isolation (dB)	ECC	Total Efficiency (%)	Size ($L \times W \times H$ mm^3)
[25]	3.6–4.7	> 11	< 0.08	87–96	9×9
[26]	3.3–3.6, 4.8–5.0	> 14	< 0.016	72–81	$12 \times 12 \times 7$
[27]	3.3–6	> 12.1	< 0.2	50–61	$22 \times 1 \times 4.3$
[28]	3.3–3.8, 4.4–7.5	> 12.9	< 0.18	60–90	$23 \times 5 \times 2.3$
[29]	3.4–5.8	> 12	< 0.11	50–82	$9 \times 2 \times 7.8$
[30]	3.4–3.6	> 16.7	< 0.1	54–65	$2 \times 60.4 \times 0.8$
[31]	2–5.2	> 10	< 0.01	72–75	$17.5 \times 2 \times 7.8$
[32]	3.2–5.9	> 11	< 0.05	\	$19.3 \times 6 \times 7.2$
Proposed	3.4–6.5	> 15	< 0.016	91–97	9.25×10.5

lation greater than 15 dB, ranking second only to the antenna in [30]. Furthermore, compared to the antennas in Table 1, the designed antenna demonstrates significant advantages in terms of ECC and efficiency. Moreover, the design based on the slot antenna on the ground plane eliminates the need for a mobile phone frame, making it suitable for smartphones with non-metal frames. Finally, the proposed MIMO antenna system also covers part of the 6 GHz frequency band, meaning that the proposed design can not only be used for multi-band applications in 5G smartphones but also accommodate the development of future 6G mobile communications.

6. CONCLUSIONS

This paper introduces an 8-element MIMO slot antenna specifically designed for 5G smartphones. The eight antenna elements are symmetrically distributed. The antenna is composed of an L-shaped feedline and a slotted rectangular slot integrated with a stepped impedance tuning structure (SITS), with all antenna elements monolithically integrated onto the ground plane. Additionally, an innovative "工"-shaped Defective Ground Structure (DGS) is proposed to mitigate surface wave coupling on the ground plane, achieving an isolation level exceeding -15 dB. Thanks to the excellent design of the antenna elements and the DGS, the antenna covers the 5G N77/N78/N79 bands, WLAN 5-GHz band, and parts of the highly anticipated 6 GHz band. Optimization of the antenna design was carried out using HFSS software, with results indicating that the envelope correlation coefficient of the antenna is below 0.016, and the efficiency ranges from 90% to 97%. After manufacturing the antenna prototype, measurements were conducted, showing consistency with the simulation results within the error range. Furthermore, this paper delves into the impact of user interaction on handheld smartphones. Based on these findings, the proposed 8-element slot antenna holds great promise for applications in 5G smartphones.

ACKNOWLEDGEMENT

This work was supported in part the Natural Science Research Project of Anhui Educational Committee under grant No. 2022AH051583, No. 2022AH052138 and No. 2023AH052650, in part by the Anhui Province Graduate Academic Innovation Project under grant No. 2023xscx074, in part by the Funding Project of Scientific Research Starting for the High-level Talents of West Anhui University under grant No. WGKQ2022009.

REFERENCES

[1] Sghaier, N., L. Latrach, and A. Gharsallah, "Design of a dual-polarized UWB 5G NR antenna," *Wireless Personal Communications*, Vol. 123, No. 2, 1293–1310, 2022.

[2] Jaglan, N., S. D. Gupta, B. K. Kanaujia, and M. S. Sharawi, "10 element sub-6-GHz multi-band double-T based MIMO antenna system for 5G smartphones," *IEEE Access*, Vol. 9, 118 662–118 672, 2021.

[3] 3GPP, "3GPP specification series: 38 series," 3GPP TS 38.101-1 v15.0.0, 2017.

[4] Yang, B., Y. Xu, J. Tong, Y. Zhang, Y. Feng, and Y. Hu, "Tri-port antenna with shared radiator and self-decoupling characteristic for 5G smartphone application," *IEEE Transactions on Antennas and Propagation*, Vol. 70, No. 6, 4836–4841, 2022.

[5] Hu, W., Z. Chen, L. Qian, L. Wen, Q. Luo, R. Xu, W. Jiang, and S. Gao, "Wideband back-cover antenna design using dual characteristic modes with high isolation for 5G MIMO smartphone," *IEEE Transactions on Antennas and Propagation*, Vol. 70, No. 7, 5254–5265, 2022.

[6] Chang, L., Y. Yu, K. Wei, and H. Wang, "Polarization-orthogonal co-frequency dual antenna pair suitable for 5G MIMO smartphone with metallic bezels," *IEEE Transactions on Antennas and Propagation*, Vol. 67, No. 8, 5212–5220, 2019.

[7] Li, Y., C.-Y.-D. Sim, Y. Luo, and G. Yang, "High-isolation 3.5 GHz eight-antenna MIMO array using balanced open-slot antenna element for 5G smartphones," *IEEE Transactions on Antennas and Propagation*, Vol. 67, No. 6, 3820–3830, 2019.

[8] Sun, L., Y. Li, Z. Zhang, and H. Wang, "Self-decoupled MIMO antenna pair with shared radiator for 5G smartphones," *IEEE Transactions on Antennas and Propagation*, Vol. 68, No. 5, 3423–3432, 2020.

[9] Ren, A., Y. Liu, H.-W. Yu, Y. Jia, C.-Y.-D. Sim, and Y. Xu, "A high-isolation building block using stable current nulls for 5G smartphone applications," *IEEE Access*, Vol. 7, 170 419–170 429, 2019.

[10] Xu, H., S. S. Gao, H. Zhou, H. Wang, and Y. Cheng, "A highly integrated MIMO antenna unit: Differential/common mode design," *IEEE Transactions on Antennas and Propagation*, Vol. 67, No. 11, 6724–6734, 2019.

[11] Zhao, A. and Z. Ren, "Size reduction of self-isolated MIMO antenna system for 5G mobile phone applications," *IEEE Antennas and Wireless Propagation Letters*, Vol. 18, No. 1, 152–156, 2019.

[12] Deng, C., D. Liu, and X. Lv, "Tightly arranged four-element MIMO antennas for 5G mobile terminals," *IEEE Transactions on Antennas and Propagation*, Vol. 67, No. 10, 6353–6361, 2019.

[13] Xu, H., H. Zhou, S. Gao, H. Wang, and Y. Cheng, "Multimode decoupling technique with independent tuning characteristic for mobile terminals," *IEEE Transactions on Antennas and Propagation*, Vol. 65, No. 12, 6739–6751, 2017.

[14] Alja'Afreh, S. S., B. Altarawneh, M. H. Alshamaileh, E. R. Almajali, R. Hussain, M. S. Sharawi, L. Xing, and Q. Xu, "Ten antenna array using a small footprint capacitive-coupled-shorted loop antenna for 3.5 GHz 5G smartphone applications," *IEEE Access*, Vol. 9, 33 796–33 810, 2021.

[15] Zhao, X., S. P. Yeo, and L. C. Ong, "Decoupling of inverted-F antennas with high-order modes of ground plane for 5G mobile MIMO platform," *IEEE Transactions on Antennas and Propagation*, Vol. 66, No. 9, 4485–4495, 2018.

[16] Barani, I. R. R., K.-L. Wong, Y.-X. Zhang, and W.-Y. Li, "Low-profile wideband conjoined open-slot antennas fed by grounded coplanar waveguides for 4×4 5G MIMO operation," *IEEE Transactions on Antennas and Propagation*, Vol. 68, No. 4, 2646–2657, 2020.

[17] Hu, W., Q. Li, H. Wu, Z. Chen, L. Wen, W. Jiang, and S. Gao, "Dual-band antenna pair with high isolation using multiple orthogonal modes for 5G smartphones," *IEEE Transactions on Antennas and Propagation*, Vol. 71, No. 2, 1949–1954, 2023.

[18] Yuan, X.-T., W. He, K.-D. Hong, C.-Z. Han, Z. Chen, and T. Yuan, "Ultra-wideband MIMO antenna system with high element-isolation for 5G smartphone application," *IEEE Access*, Vol. 8, 56 281–56 289, 2020.

[19] Hei, Y. Q., J. G. He, and W. T. Li, "Wideband decoupled 8-element MIMO antenna for 5G mobile terminal applications," *IEEE Antennas and Wireless Propagation Letters*, Vol. 20, No. 8, 1448–1452, 2021.

[20] Ahn, J., Y. Youn, B. Kim, J. Lee, N. Choi, Y. Lee, G. Kim, and W. Hong, "Wideband 5G N77/N79 4×4 MIMO antenna featuring open and closed stubs for metal-rimmed smartphones with four slits," *IEEE Antennas and Wireless Propagation Letters*, Vol. 22, No. 12, 2798–2802, 2023.

[21] Sun, L., Y. Li, and Z. Zhang, "Wideband decoupling of integrated slot antenna pairs for 5G smartphones," *IEEE Transactions on Antennas and Propagation*, Vol. 69, No. 4, 2386–2391, 2021.

[22] Cheng, B. and Z. Du, "A wideband low-profile microstrip MIMO antenna for 5G mobile phones," *IEEE Transactions on Antennas and Propagation*, Vol. 70, No. 2, 1476–1481, 2022.

[23] Sun, L., Y. Li, and Z. Zhang, "Wideband integrated quad-element MIMO antennas based on complementary antenna pairs for 5G smartphones," *IEEE Transactions on Antennas and Propagation*, Vol. 69, No. 8, 4466–4474, 2021.

[24] Chen, Z., Y. Liu, T. Yuan, and H. Wong, "A miniaturized MIMO antenna with dual-band for 5G smartphone application," *IEEE Open Journal of Antennas and Propagation*, Vol. 4, 111–117, 2023.

[25] Wang, Z., W. You, M. Yang, W. Nie, and W. Mu, "Design of MIMO antenna with double L-shaped structure for 5G NR," *Symmetry*, Vol. 15, No. 3, 579, 2023.

[26] Ren, W., Z. Wang, W. Nie, W. Mu, C. Li, M. Wang, and W. You, "A 12-unit asymmetric mirror-coupled loop antenna for 5G smartphones," *Progress In Electromagnetics Research C*, Vol. 145, 141–152, 2024.

[27] Ren, A., H. Yu, L. Yang, Z. Huang, Z. Zhang, and Y. Liu, "A broadband MIMO antenna based on multimodes for 5G smartphone applications," *IEEE Antennas and Wireless Propagation Letters*, Vol. 22, No. 7, 1642–1646, 2023.

[28] Lin, H., W. Sun, Z. Wang, and W. Nie, "A dual-band MIMO antenna based on multimode for 5G smartphone applications," *Progress In Electromagnetics Research C*, Vol. 148, 31–42, 2024.

[29] Chen, H.-D., Y.-C. Tsai, C.-Y.-D. Sim, and C. Kuo, "Broadband eight-antenna array design for sub-6 GHz 5G NR bands metal-frame smartphone applications," *IEEE Antennas and Wireless Propagation Letters*, Vol. 19, No. 7, 1078–1082, 2020.

[30] Fang, Y., Y. Jia, J.-Q. Zhu, Y. Liu, and J. An, "Self-decoupling, shared-aperture, eight-antenna MIMO array with MIMO-SAR reduction," *IEEE Transactions on Antennas and Propagation*, Vol. 72, No. 2, 1905–1910, 2024.

[31] Wang, Z., M. Li, M. Yang, W. Nie, W. Mu, H. Lin, and Z. Lu, "Design of wideband 8-element MIMO mobile phone antenna based on sub-6 GHz NR band," *Progress In Electromagnetics Research C*, Vol. 129, 187–201, 2023.

[32] Chen, Z., M. Ye, Z. Zhang, and X. Wu, "A wideband MIMO antenna with shared radiator for 5G smartphones," in *2024 IEEE MTT-S International Wireless Symposium (IWS)*, 1–3, Beijing, China, 2024.